PSI-SR-1229

Advanced Diagnostics and Kinetics of Oxygen-Iodine Laser Systems

Wilson T. Rawlins
Seonkyung Lee
William J. Kessler
Lawrence G. Piper
Steven J. Davis

Wilson T. Rawlins, Seonkyung Lee, William J. Kessler, Lawrence G. Piper, Steven J. Davis, "Advanced Diagnostics and Kinetics of Oxygen-Iodine Laser Systems ," presented at 36th AIAA Plasmadynamics and Lasers Conference (Toronto, Ontario, Canada), (6-9 June2005).

Advanced Diagnostics and Kinetics of Oxygen-Iodine Laser Systems

Wilson T. Rawlins,[*] Seonkyung Lee,[†] William J. Kessler,[‡] Lawrence G. Piper,[§] and Steven J. Davis[**]
Physical Sciences Inc., Andover, MA 01810-1077

This paper describes a comprehensive, multispecies diagnostic suite for the characterization of chemical and electrical oxygen-iodine laser kinetics. Oxygen-iodine lasers involve reactions and energy transfer among several key species, including electronically excited O_2(a) and O_2(b), the reagent I_2, ground-state I, electronically excited I^*, and, in the case of electric-discharge driven systems, atomic oxygen. We have implemented highly sensitive and accurate methods for the measurement of all of these species in a chemically reacting flow system. We have used quantitative near-infrared emission spectroscopy to detect O_2(a), O_2(b), and I^*, ultra-high precision absorption spectroscopy to detect I_2, ultra-high precision tunable diode laser absorption spectroscopy to detect $I:I^*$ small-signal gain, and a chemiluminescent titration method to detect O. All of these methods provide well-resolved species concentrations, and the spectral emission and laser absorption measurements also provide spectroscopic determinations of gas temperature. Multispecies measurements of this type constrain reacting flow models so that gaps in our understanding of these systems can be identified and resolved. Through accurately calibrated spectral emission measurements, we have shown that high yields of O_2(a) (>20%) can be attained via microwave discharge excitation of flowing dilute mixtures of O_2 and Ar. For these conditions, we have observed positive small-signal gain on the I^* - I transition, however the multispecies concentration data clearly show the existence of previously unknown kinetics limitations related to the presence of O. We discuss the calibration and accuracy of the diagnostic methods, and the implications of the results for the kinetics of discharge-driven oxygen-iodine laser systems.

I. Introduction

The production of $O_2(a^1\Delta_g)$ by electric discharge of flowing oxygen gas mixtures is an attractive approach to energy transfer excitation and lasing of the $I(^2P_{1/2}) \rightarrow I(^2P_{3/2})$ transition at 1.315 μm. The near-resonant chemi-excitation of $I(^2P_{1/2})$ (or I^*) emission in the reaction of $O_2(a^1\Delta)$ with I_2 is well known,[1,2] and is the basis for the Chemical Oxygen-Iodine Laser (COIL).[3,4] This device uses an aqueous chemical process to generate $O_2(a^1\Delta)$, and relies on multi-step energy transfer between singlet molecular oxygen and I_2 to produce I. The potential for gas-phase electric discharge generation of $O_2(a^1\Delta)$ to produce $I(^2P_{1/2}) \rightarrow I(^2P_{3/2})$ lasing offers substantial improvements in efficiency and weight limitations of closed-cycle systems.

A major mechanistic difference between the discharge and chemical methods is the discharge's prolific production of O from the electron-impact dissociation of the O_2 feedstock. O reacts rapidly with I_2 to form IO, which in turn reacts rapidly with O to form I,[5] so that essentially no $O_2(a^1\Delta)$ is consumed in I_2 dissociation. Previous kinetics investigations of the oxygen-iodine system using discharge-generated $O_2(a^1\Delta)$ employed catalytic recombination of O,[1,2] and thus did not examine conditions relevant to a discharge-driven laser system. As a result, very little is known about the abundances and effects of the discharge effluent species relevant to I^* excitation.

[*] Principal Research Scientist, Physical Sciences Inc., 20 New England Business Center, Andover, MA 01810, and Member.
[†] Principal Scientist, Physical Sciences Inc., 20 New England Business Center, Andover, MA 01810.
[‡] Principal Research Scientist, Physical Sciences Inc., 20 New England Business Center, Andover, MA 01810.
[§] Principal Research Scientist, Physical Sciences Inc., 20 New England Business Center, Andover, MA 01810.
[**] VP, Applied Optics Enterprise, Physical Sciences Inc., 20 New England Business Center, Andover, MA 01810, and Member.

Recently, Carroll and coworkers reported the first observations of $I^* \rightarrow I$ gain[6] and lasing[7] from discharge-generated $O_2(a^1\Delta)$ and O, using supersonic expansion to achieve positive gain at low temperatures.[8] We have recently reported similar observations of positive $I^* \rightarrow I$ gain in a subsonic, microwave-discharge flow reactor near room temperature.[9] In the present paper, we describe results from a series of kinetics investigations of the production of $O_2(a^1\Delta)$ and O by a conventional microwave discharge at a few torr, and of the subsequent interactions with I_2 reagent near room temperature. The experiments are based on a multispecies measurement approach, using a suite of high-sensitivity optical emission and absorption diagnostics to determine time-resolved, absolute species concentrations for $O_2(a^1\Delta)$, O, I_2, I^*, and I, as well as small-signal gain and temperature.[10,11]

For typical O concentrations produced in a flow reactor by a microwave discharge at a few torr, I_2 is promptly dissociated upon addition to the flow, and the near-resonant $O_2(a^1\Delta)$ + I energy exchange is expected to attain a steady state which is essentially an equilibrium:

$$O_2(a) + I \rightleftarrows O_2(X) + I^* \tag{1}$$

$$\frac{[I^*]}{[I]} = K_{eq} \frac{[O_2(a)]}{[O_2(X)]} \ , \ K_{eq} = 0.75 \exp(402 / T) \tag{2}$$

This expression holds if the quenching of I^* by O is negligible, i.e. $k_{I^*+O}[O] \lesssim k_{I^*+O2}[O_2(X)]/10$. For the experimental conditions given below, this corresponds to $k_{I^*+O} < 6 \times 10^{-12}$ cm^3/molecule-s, and is consistent with $k_{I^*+O} \lesssim 2 \times 10^{-12}$ cm^3/molecule-s recently measured by Heaven and coworkers.[12] Thus the $[O_2(a)]/[O_2(X)]$ ratio required to achieve the threshold for positive gain, $[I^*]/[I] = 0.5$, should be given by the equilibrium expression and decreases with temperature. $[O_2(X)]$ is given by

$$[O_2(X)] = [O_2]_o - [O_2(a)] - [O]/2 \tag{3}$$

where $[O_2]_o$ is the total O_2 concentration, and the yield of $O_2(a)$ is defined as $[O_2(a)]/[O_2]_o$. (Note that we expect O_3 to be a negligible component of the discharge effluent for our experimental conditions.) The value of $[O_2]_o$ is determined from the mole fraction of O_2 admitted to the discharge, and the pressure and temperature of the $O_2(a)$ + I reaction zone. For 15% dissociation of the initial O_2, the expected threshold $O_2(a)$ yields are 0.126 and 0.167 at 300 K and 400 K, respectively. As [O] decreases toward zero, these values approach upper bounds of 0.149 at 300 K and 0.196 at 400 K. Thus, according to Eq. (2), $O_2(a)$ yields in excess of 0.2 should give rise to positive $I^* \rightarrow I$ optical gain upon addition of I_2 near room temperature.

II. Excitation of $O_2(a^1\Delta)$ in a Microwave Discharge

$O_2(a)$ can be generated efficiently in a variety of electric discharge types and configurations. In this work we have used a conventional, electrodeless microwave discharge at 2450 MHz with a tuned, resonant cavity of the Evenson design.[13] This type of cavity operates on gas flows through a 13-mm o.d. pyrex or quartz tube, at typical pressures from about 0.5 torr to about 20 torr, and externally applied powers up to ~120 W. The chemistry of low-pressure, resonant-cavity microwave discharges is described by Kaufman.[14] The externally applied electric field strength is nominally ~30 V/cm. The electron number density is in the 10^{11} to 10^{12} cm^{-3} range, and is limited primarily by wall losses and dissociative recombination. The wall loss is accentuated by the Debye shielding effect, which confines most of the ion-pair production to an axisymmetric annular region near the inner surface of the glass tube. The gas temperature within the discharge is usually about 500 to 600 K for an air-cooled pyrex tube. For 3 torr, 500 K, and ~70 W discharge power, the electric field parameter E/N is ~(5 to 10) x 10^{-16} V cm^2, or 50-100 Td (where E is the electric field strength and N is the total number density). The characteristic electron energy (electron diffusion/mobility ratio) ranges from ~2 eV for a diatomic gas to ~8 eV for a monatomic rare gas like argon. The electron energy distributions follow a non-Boltzmann distribution, i.e. the high-energy tail of the distribution is suppressed due to inelastic collisions with the gas molecules. Ionization levels are typically low, diffusion is ambipolar, and the ions and electrons recombine promptly upon leaving the active discharge.

We have previously published model calculations of excitation rates in O_2/Ar discharges.[15] The rate coefficients for the electron-impact excitation processes are given by the convolution integral of the energy-dependent excitation cross sections and the electron energy distribution. To calculate these, we used a computer code[16] which solves the Boltzmann transport equation.[17] The code treats all the inelastic processes occurring in the active discharge, to evaluate the steady-state electron energy distributions and reaction rate coefficients as functions of E/N and O_2 mole

fraction in Ar or He. The electron-impact cross section data are taken from the data base discussed extensively by Phelps and co-workers.[18-20] The calculations and data base are discussed in detail in Reference 15.

The effects of E/N and O_2 mole fraction on the computed electron energy distributions are shown in Figure 1. With either increasing E/N or decreasing O_2 fraction, the fraction of high-energy electrons increases, signifying increasing electron "temperature". The increases in the high-energy component of the electron energy distribution result in larger overlap integrals with the key electronic excitation cross sections, illustrated in Figure 2. The 10 Td distribution provides power-efficient $O_2(a)$ excitation, in that very little power is expended on O_2 dissociation; however the poor overlap with the ionization cross section results in a very low ionization rate and consequently low electron number density. The 100 Td distribution gives greater overlap with both the $O_2(a)$ excitation cross section and the O_2 ionization cross section, but at the expense of increased O_2 dissociation. The $O_2(a)$ excitation rate is given by the product $k_{exc}[e^-][O_2]$. Both k_{exc} and $[e^-]$, and hence the yield of $O_2(a)$, can be considerably enhanced through use of larger E/N and/or lower O_2 mole fraction to achieve more energetic electron energy distributions.

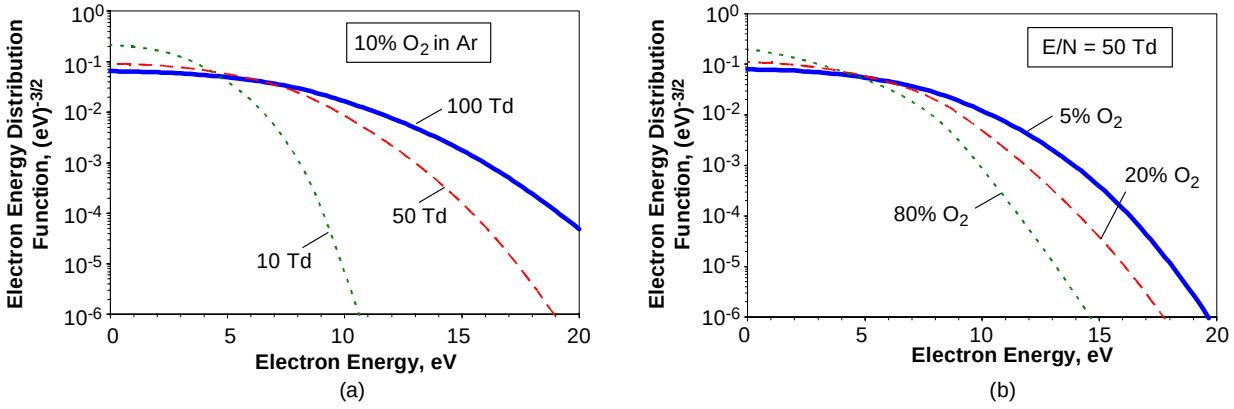

Figure 1. Computed electron energy distribution functions in discharge-excited O_2/Ar mixtures: (a) Effect of variations in E/N for 10% O_2 in Ar; (b) Effect of variations in O_2 mole fraction for E/N = 50 Td.

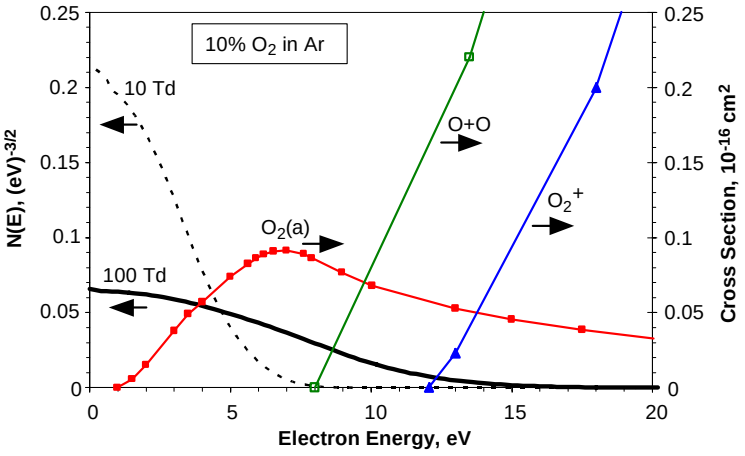

Figure 2. Illustration of overlap of electron energy distributions with electron impact excitation cross sections for $O_2(a)$ excitation, O_2 dissociation to form O + O, and O_2 ionization to form O_2^+. The electron energy distributions are computed for E/N = 10 and 100 Td, in 10% O_2/Ar. Cross section values were taken from Ref. 20.

The computed dependences of the rate coefficients for $O_2(a)$ excitation, O_2 dissociation, and O_2 ionization on O_2 mole fraction in Ar are shown in Figure 3 for E/N = 50 Td. The excitation rate coefficient increases modestly with decreasing O_2 fraction. However, the O_2 ionization rate coefficient increases by almost two orders of magnitude from 80% O_2 to 5% O_2, signifying a large increase in the ion pair production rate and in the electron number density. The Ar ionization rate coefficient, which has a higher energy threshold, is even more sensitive to the O_2 fraction, and becomes an important contributor for the dilute mixtures. For the discharge configuration and flow rates used in the experiments reported here, the gas residence time in the discharge is ~0.2 ms. This corresponds to an effective $O_2(a)$ "loss" rate which is faster than the collisional losses within the discharge for our anticipated electron number densities. To zeroth order, we can approximate the $O_2(a)$ production as

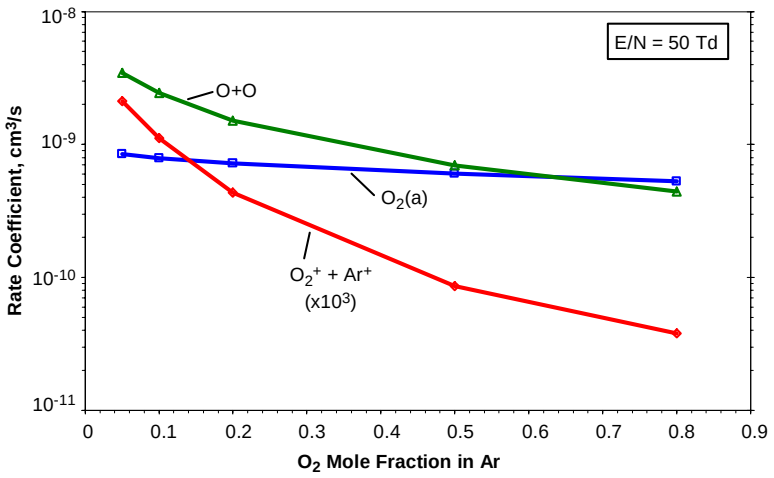

Figure 3. Effect of variations in O_2 mole fraction on computed electron-impact rate coefficients for O_2(a) excitation, O_2 dissociation, and total ionization for discharge-excited O_2/Ar mixtures, E/N = 50 Td.

$$[O_2(a)] \;.\; k_{exc}[e^-][O_2]\tau \;, \quad (4)$$

where τ denotes the gas residence time in the discharge. The O_2(a) yield is then simply $\sim k_{exc}[e^-]\tau$, and is thus highly dependent on the electron energy distribution via E/N and O_2 fraction. Of course, a quantitative treatment requires inclusion of the O_2(a) losses due to collisions with electrons (superelastic quenching, dissociation), as well as the effects of dissociative attachment of electrons with O_2 and the subsequent role of O^-.[21,22] (Note that deactivation of O_2(a) by collisions with the reactor walls and with neutral discharge species in and downstream of the discharge is negligible for our experimental conditions.) This analysis, coupled with continuing measurements with different residence times, is in progress.

III. Experimental Methods and Optical Diagnostics

The experiments were performed in a conventional discharge-flow reactor shown in Figure 4. The primary flow was a mixture of 5% to 80% O_2 in Ar at 1.5 and 3 torr. The gas passed through a 2450 MHz microwave discharge excited by an Evenson-style resonant cavity[13] at 40 to 120 W power, with an approximate residence time of 0.2 ms in the active discharge. Flow velocities in the main flow tube (5 cm o.d.) were 1100-1300 cm/s. For investigations of I^* excitation, I_2 was added at trace concentrations by passing Ar over a bed of iodine crystals at room temperature and through a ¼-inch (o.d.) pyrex sliding injector. I_2 flow rates were determined by optical absorption using a light-emitting diode filtered at 488 nm.[23] Initial I_2 concentrations in the flow reactor were (5 to 12) x 10^{12} molecules/cm^3. Additional reagents, NO and NO_2, were added through a fixed loop injector 16 cm (~13 ms) upstream of the optical port. Typical flow times from the discharge exit to the optical cell were ~20 ms. Typical concentrations of O and O_2(a) were on the order of $10^{14\text{-}15}$ molecules/cm^3.

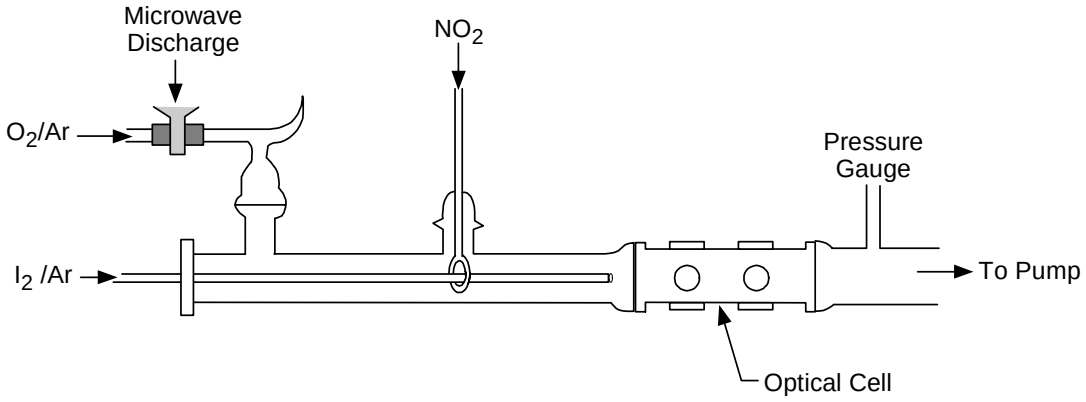

Figure 4. Schematic diagram of discharge-flow reactor apparatus.

The optical measurements were performed concurrently along two orthogonal sight paths at the first window station of the optical cell. Absorption and gain on the I($^2P_{3/2}$, F=4) – I($^2P_{1/2}$, F=3) hyperfine transition were observed by a narrow-band (<10 MHz full width at half maximum) frequency-scanning diode laser at 1.315 μm, in a fiber-coupled, dual-beam configuration.[10,11,24] The measurements used a single pass of the laser beam across the 5.6 cm diameter of the optical cell. A balanced ratiometric detection circuit[25] provided noise cancellation and ultra-high

sensitivity. Analysis of the Doppler-broadened line shapes gave gas temperatures of 330-350 K. Division of the negative absorbance, $-\ln(I_o/I)$, by the path length gives the small-signal gain in cm^{-1}; division of this quantity by the stimulated emission cross section gives the quantity $[I^*] - [I]/2$. We also attempted to make the measurements with a multipass (~40 passes) Herriott cell arrangement, however we observed discrepancies between the single-pass and multipass results that were apparently due to the effects of radial concentration gradients in I and/or I^* across the off-axis lines of sight of the multipass beam path. Such radial gradients occur for species which are efficiently removed or deactivated at the reactor wall, as expected for I^* and possibly for I as well.

Emission spectra from $O_2(a^1\Delta_g \rightarrow X^3\Sigma_g^-$, 1270 nm) and $I(^2P_{1/2} \rightarrow {}^2P_{3/2}$, 1315 nm) were observed with a liquid-nitrogen-cooled InGaAs array spectrometer at 0.5 nm resolution.[10,11] The emission was collected by an optical fiber mounted on the entrance slit. The field of view was collimated and apertured to view only the opposing window, with no reflecting surfaces. The instrument was calibrated for absolute spectral responsivity to "1% accuracy using a NIST traceable blackbody source. All windows were antireflection-coated for 1.3 μm, and the windows for the emission measurements were purged with a small flow of Ar to prevent deposition of iodine oxides. O concentrations were determined to "5% accuracy using the O + NO titration method,[26-28] where the continuum air-afterglow emission from the O + NO interaction was viewed by a calibrated, bandpass-filtered photomultiplier at 580 nm. NO used in these determinations was purified of higher oxides by passage through an Ascarite trap (NaOH supported on asbestos) followed by an alcohol/liquid nitrogen slush trap, was diluted in He, and was stored in a Pyrex vacuum bulb.

The emission spectra of $O_2(a \rightarrow X)$ and $I^* \rightarrow I$ were corrected for detector baselines and were converted into absolute column intensities, photons/cm^2-s-sr-nm, using the spectral responsivities determined by blackbody calibrations of the full spectrometer optical collection system. An example $O_2(a \rightarrow X)$ spectrum is shown in Figure 5, together with a spectrum computed by a least squares spectral fitting procedure. The spectral fitting analysis gives a rotational temperature of 350 K, in excellent agreement with temperatures determined from the $I \rightarrow I^*$ absorption line widths when I_2 is injected. In addition, the analysis confirms that all of the observed emission is due to the (0,0) band of the $a \rightarrow X$ system, i.e. there is no observable vibrational excitation of the $O_2(a)$ 20 ms downstream of the discharge. Consequently, $O_2(a)$ concentrations can be accurately determined by integration of the spectra and application of the Einstein A-coefficient for the band. Both the spectral fitting and band-integral methods are based on the fundamental principle relating emission intensity and upper state number density:[29]

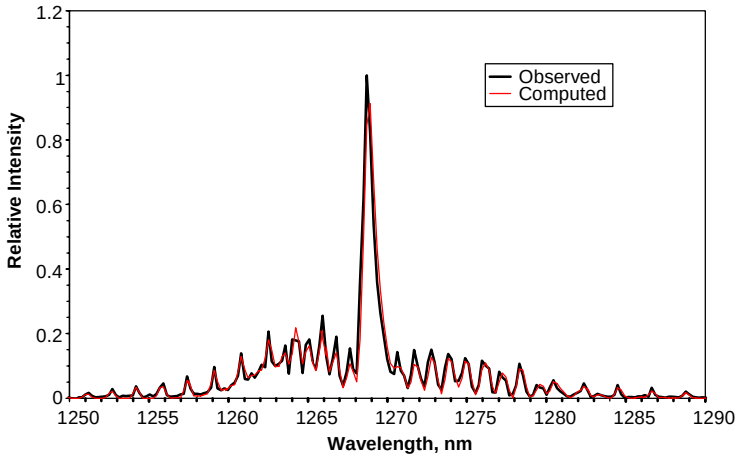

Figure 5. Observed and best-fit computed spectra for $O_2(a \rightarrow X)$ emission: microwave discharge of O_2 at 2.6 torr, spectral resolution 0.5 nm, rotational temperature 350 K.

$$(4\pi/\Re) \int I(\lambda)d\lambda = N_u A_{ul} \quad , \tag{5}$$

where $\Re$ is the path length across the viewing volume (5.6 cm), $I(\lambda)$ denotes the set of spectral column intensities over the entire band, 4π is the solid angle (in sr) for isotropic, optically thin molecular emission, N_u is the number density of the upper or emitting state, and A_{ul} is the Einstein coefficient for the transition. From the responsivity calibrations, the product $N_u A_{ul}$ is determined to a relative uncertainty of about "2%. Although the Einstein coefficient for the $O_2(a \rightarrow X)$ transition has been the subject of considerable controversy and uncertainty in the past, recent determinations by two independent groups and three independent methods indicate a value of 2.2×10^{-4} s^{-1} with an overall relative uncertainty of "10%.[30,31] The net relative uncertainty of our $[O_2(a)]$ determination is then a systematic error of "10%. Combining the uncertainty in $[O_2]_o$ as determined from the measured flow rates, pressures, and gas temperatures, the net relative uncertainty in the $O_2(a)$ yield is "14%. Similarly, $[I^*]$ is determined with "20% relative uncertainty by integration of the spectrum and application of the Einstein coefficient, 8.0 " 1.6 s^{-1}.[32]

In separate measurements, we confirmed ~100% fractional dissociation of I_2 in the O + I_2 and O + IO reaction sequence:[10]

$$O + I_2 \rightarrow IO + I \quad (6)$$
$$O + IO \rightarrow O_2 + I \quad (7)$$

For the O concentrations in our experiments, we expect prompt, complete dissociation of I_2 by O, essentially as rapidly as the injected I_2 can be mixed into the main flow. We performed direct measurements of I_2 in absorption using a high-precision, 21-bit absorption photometer.[10] This sensor uses an LED light source at 488 nm as previously described by Davis and Hanko,[23] to probe the dissociative continuum portion of the I_2 absorption spectrum.[33,34] Through use of a dual-beam optical system and a noise-cancelling electrometer circuit, the sensor can measure I_2 absorbances as small as 5 x 10^{-6} at 1 Hz.[10] This corresponds to an I_2 detection limit of 6 x 10^{11} molecules/(cm^3 $Hz^{1/2}$) in our flow reactor. This sensitivity enables the accurate determination of I_2 concentrations delivered to the reaction zone, as well as any significant unreacted I_2 in the presence of the discharge-activated oxygen. Repeated measurements for typical discharge and flow conditions ([O] > 10^{15} molecules/cm^3) confirm that, at initial flow reactor concentrations of ~5 x 10^{13} molecules/cm^3 and less, I_2 is at least 97% dissociated within reaction times of 10 ms or less. In addition, measurements of [I^*] by emission and [I^*] – [I]/2 by laser absorption can be combined to determine [I^*] and [I], providing an independent assessment of the fractional I_2 dissociation. For reagent mixing/reaction times >4 ms, the initially injected [I_2] agreed with the observed ([I^*]+[I])/2 to ~10%, confirming the calibration of the emission spectrometer. For reaction times <4 ms, the I_2 was only partially dissociated, an indication of incomplete mixing for these short flow distances.

IV. Results and Analysis

A. O and O_2(a) Yields

We have determined atomic oxygen and O_2(a) yields for our Evenson-cavity microwave discharge-flow reactor (Figure 4) as a function of power and O_2 mole fraction in argon diluent. The measurements were performed at two pressures, 1.5 and 3 torr, and linear flow velocities of about 1300 cm/s. In these measurements, we took care to maintain constant linear flow velocity as the pressure and O_2 mole fraction were changed, in order to ensure a constant residence time of ~0.2 ms in the active discharge. Thus the observed variations in O and O_2(a) yields reflect variations in their respective electron-impact dissociation/excitation rate coefficients and the electron number density (i.e. ionization rate) with changing electron energy distributions. Variations with discharge power at constant pressure and O_2 mole fraction should reflect primarily changes in the electric field strength and electron number density within the discharge.

Typical observed O-atom concentrations were in the range (0.7 to 2) x 10^{15} molecules/cm^3. Measurements of the air-afterglow intensity along the length of the flow tube confirmed that there was negligible loss of O due to heterogeneous and homogeneous recombination, as we expected. Atomic oxygen yields, expressed as $[O]/[O_2]_o$, are plotted as a function of discharge power in Figure 6; the power dependence was observed for 1.5 torr, 5.4% O_2 and 3 torr, 5.1% O_2. The air-afterglow determinations were highly reproducible, to within 5% or less. The curves are quadratic fits to the data. The atomic oxygen yield increases a factor of 1.6 to 2.3 for a factor of 3 increase in the discharge power. The variation of O yield with initial O_2 mole fraction for 1.5 and 3 torr, at 70 W discharge power, is shown in Figure 7. In this case, the O yield variation is approximately inverse-first order in O_2 mole fraction, approaching 0.4 (20% O_2 dissociation) at 5% O_2 and 1.5 torr. The observed O yields exhibit small variations from day to day, apparently due to slight variations in the details of the discharge cavity configuration, tuning, and air cooling.

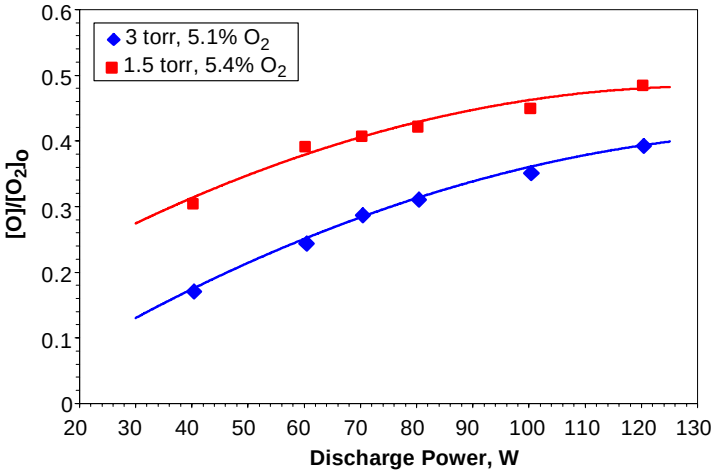

Figure 6. Dependence of atomic oxygen yield on microwave discharge power for 1.5 and 3 torr, ~5% O_2 in Ar.

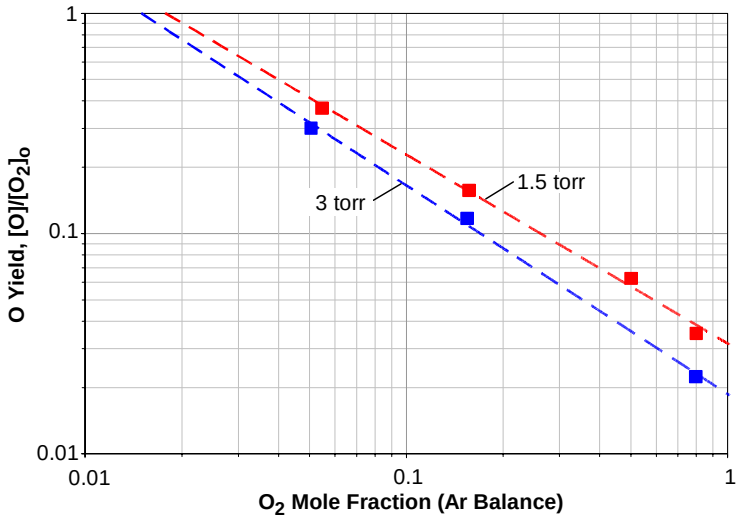

Figure 7. Dependence of atomic oxygen yield on O_2 mole fraction and total pressure: Ar diluent, 70 W discharge power, 1.5 and 3 torr.

The increase in O yield with decreasing O_2 mole fraction and decreasing pressure is consistent with our expectations based on the discharge physics outlined above.

Observed $O_2(a)$ yields as functions of O_2 mole fraction (1.5 and 3 torr) and discharge power (1.5 torr) are plotted in Figures 8 and 9, respectively. The observed $O_2(a)$ concentrations were (0.5 to 2) x 10^{15} molecules/cm^3. Measurements of the $O_2(a)$ emission intensity along the length of the flow tube confirmed that there were no significant wall or quenching losses, as expected. (O and $O_2(a)$ have similar accommodation coefficients on untreated pyrex, ~10^{-4} per collision.[35,36]) Day to day variations in the discharge behavior are illustrated in Figure 9. As in the case of O, the $O_2(a)$ yields increase with decreasing pressure, and increase markedly with decreasing O_2 mole fraction. For 5% O_2 at 1.5 torr and discharge powers of 70 W or more, we routinely observe $O_2(a)$ yields in excess of 0.2. These yields are well above the equilibrium threshold for inversion of the I^* population.

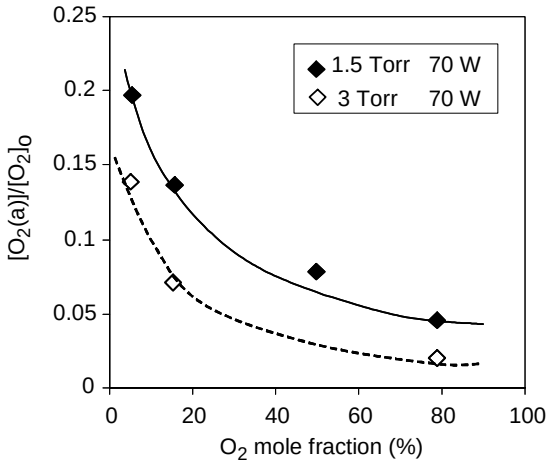

Figure 8. Dependence of $O_2(a)$ yield on O_2 mole fraction and total pressure: Ar diluent, 70 W discharge power, 1.5 and 3 torr.

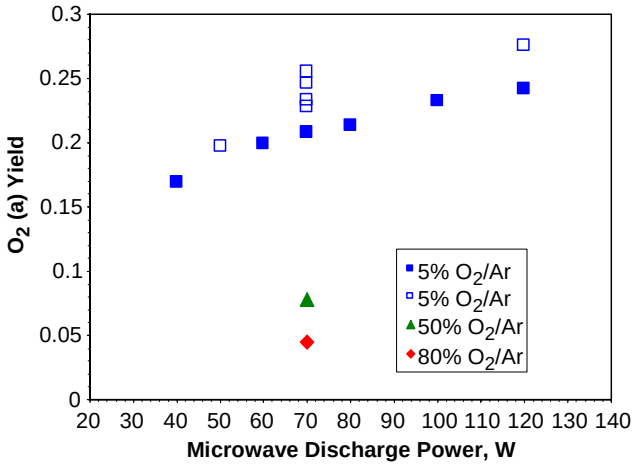

Figure 9. Dependence of $O_2(a)$ yield on microwave discharge power for 1.5 torr and three O_2/Ar mixtures. The two data sets for 5% O_2/Ar were observed on separate, consecutive days, and indicate day to day variability in the discharge operation.

For some of the experiments, we used the near-infrared spectrometer to observe $O_2(b)$ emission spectra, $O_2(b^1\Sigma_g^+ \rightarrow X^3\Sigma_g^-)$, centered at 760 nm. The responsivity of the instrument is about a factor of 5 lower at this wavelength than at 1300 nm, however the Einstein coefficient for the b→X band is almost 400 times larger than that for the a→X band, so $O_2(b)$ emission is readily detectable, even when $O_2(b)$ is present in trace amounts. $O_2(b)$ is produced in the discharge by electron-impact excitation of $O_2(X)$, with an excitation rate coefficient which is a factor of ~4 smaller than that for $O_2(a)$ excitation,[15] and is also formed from quenching of discharge-excited $O(^1D)$ by O_2.[22,37] However, unlike $O_2(a)$, $O_2(b)$ is rapidly quenched by the walls and, to some extent, by O-atoms,[38] so that its concentration in the reaction zone of the flow tube is very small. Accordingly, our measurements typically show the $O_2(b)$ concentration at the measurement cell is some two orders of magnitude below that of $O_2(a)$ and is therefore insignificant. Similarly, vibrationally excited $O_2(v)$ is produced rapidly in the discharge, however it is rapidly deactivated by collisions with O and with the reactor walls downstream of the discharge.[15,39] The same

expectation applies to the other discharge-produced metastables of O, O_2, and Ar. We expect O_3 to be present in the discharge effluent flow, but at low concentrations. Most of the O_3 reaching the reaction zone is formed downstream of the discharge by three-body recombination of O and O_2. For this process, we estimate $[O_3] < 10^{12}$ molecules/cm^3 in the flow reactor for our experimental conditions. Thus the primary discharge-produced species in the effluent flow are expected to be O and O_2(a).

As discussed above, the observed increases in O and O_2(a) production with decreasing pressure and O_2 mole fraction result from a combination of increasing electron-impact rate coefficients and increasing electron number densities, both of which result from increasing electron "temperatures" in the discharge. Much of the mole fraction effect appears to be due to greatly increased ionization rates at low mole fractions. The mole fraction effect is more pronounced for O than for O_2(a), reflecting the larger energy threshold for O_2 dissociation than for O_2(a) excitation. This is illustrated by the computed rate coefficients plotted in Figure 3, where the rate coefficient for O_2 dissociation is a steeper function of O_2 mole fraction than that for O_2(a) excitation. All of these trends are consistent with O_2/Ar discharge model predictions previously published by Rawlins et al.[15] However, we note that our observed O production, relative to that for O_2(a), is considerably less than that implied by the O_2 dissociation cross sections compiled by Phelps.[18,20] Figure 10 shows our observed $[O_2(a)]/[O]$ values, compared to the computed ratios of O_2(a) and O production rates given by $k_{exc}/2k_{diss}$. Since O_2(a) probably suffers additional electron-induced loss processes in the discharge that O does not experience, this simple ratio of the production rates provides an upper bound to the predicted concentration ratio downstream of the discharge. The data show surprisingly little pressure dependence, and a relative variation with O_2 mole fraction which is consistent with the curves for 50-100 Td. However, the observed ratios are much larger than the predicted upper bounds. Since the O_2(a) excitation cross section appears to be reasonably well determined,[19] we infer that the O_2 dissociation cross sections give a substantial overprediction of O formation, by perhaps as much as an order of magnitude. The O_2 dissociation cross section reported by Cosby[40] is smaller and tends to underpredict the O production. Clearly, this aspect of the O_2/Ar discharge modeling needs closer attention and comparison to experimental data.

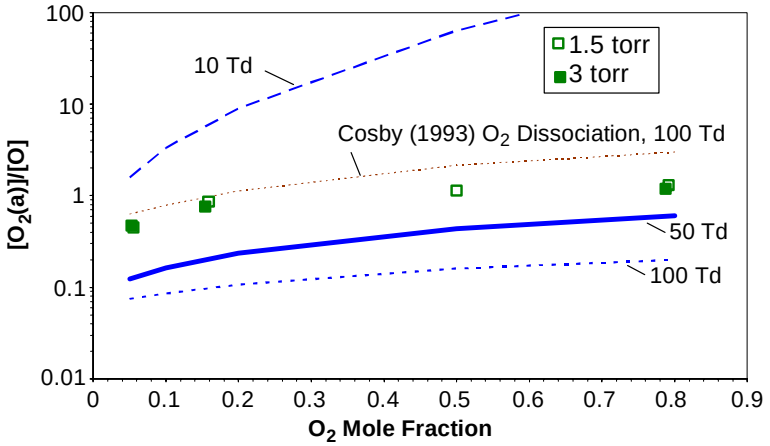

Figure 10. $[O_2(a)]/[O]$ ratios observed at 1.5 and 3 torr, compared to computed upper bounds as described in the text.

B. I^* Excitation

To investigate the kinetics of I^* excitation, we injected I_2 into the discharge effluent in the flow reactor at several distances from the observation port, to give systematic variations in the reaction time. I_2 was diluted in He and was injected at initial concentrations of (0.5 to 1.3) x 10^{13} molecules/cm^3, so that [O] and $[O_2(a)]$ were well in excess. The discharge conditions were (5 to 80)% O_2 in Ar at 1.5 and 3 torr and 40-120 W, however we emphasized 5% O_2 at 1.5 torr and 70-120 W where the O_2(a) yields were highest. For these conditions, the lifetime of I_2 against reaction with O is <<0.1 ms, so the rate of I_2 dissociation is limited by mixing of the injectant gas with the main flow stream. All of the I_2 dissociation occurs through the reactions of I_2 and IO with O. This takes place so rapidly that the multi-step O_2(a) + I_2 energy transfer sequence, which is the usual I_2 dissociation mechanism in the absence of O (as in COIL reactors),[2] does not occur, and no O_2(a) can be consumed by this path. The reacting mixture then consists of excess O and O_2(a), with much smaller concentrations of I and I^*; this mixture flows down the reactor from the reagent inlet to the observation port. These expectations are borne out by observations of the emission spectra of $O_2(a \rightarrow X)$, $O_2(b \rightarrow X)$, and $I^* \rightarrow I$, with no detectable emission from the $I_2(A^3\Pi \rightarrow X^1\Sigma)$ or $I_2(B^3\Pi \rightarrow X^1\Sigma)$ bands, which would be excited in the multi-step O_2(a) + I_2 energy transfer sequence.[2] We observed a faint, visible $I_2(B \rightarrow X)$ flame immediately downstream of the injector, which extended only for about 1-2 cm as the I_2 was consumed.

Addition of small concentrations of I_2 gave rise to strong I^* emission at 1315 nm and net $I \rightarrow I^*$ absorption of the scanning diode laser beam (negative small-signal gain). We observed net absorption even for cases where the initial O_2(a) yield was well above the equilibrium threshold for positive gain. This occurs in part because the addition of I_2 results in significant depletion of $[O_2(a)]$, even though the injected I_2 concentrations are ~100 times smaller than

those of $O_2(a)$. In addition, we observed net absorption even when the depleted $O_2(a)$ yield was observed to be essentially at the threshold, where the medium should be near transparency. These results indicate a complex quenching effect which calls into question the equilibrium description of I^* excitation given by (1) and (2).

Example traces of the scanning laser absorption/gain measurement are shown in Figure 11, for cases with and without the addition of I_2 at 1.5 torr, 5% O_2 in Ar, 70 W power, 350 K. Prior to the injection of I_2, the $O_2(a)$ yield measured from the near-infrared emission was 0.25 ($[O_2(a)]$ = 5.2 x 10^{14} molecules/cm^3), and the upper curve was observed, corresponding to zero gas-phase absorption. Upon injection of I_2 at an initial concentration of 6 x 10^{12} molecules/cm^3, with a reaction time of 12 ms from the injector to the observation port, the observed $O_2(a)$ yield promptly diminished to 0.17 ($[O_2(a)]$ = 3.5 x 10^{14} molecules/cm^3) and a clear absorption signal was observed, corresponding to a net negative small-signal gain of -2.3 x 10^{-3} %/cm at line center. For these measurements, the laser was scanned repeatedly across the transition at 50 Hz, and 1000 scans were averaged for each of the traces shown. The traces are clearly affected by etalons in the optical system (e.g. due to non-wedged windows and to reflections between the beam launch and collection optics) which are commonly observed at these very low signal levels. Accordingly, we processed the averaged absorption spectra by fast Fourier transform filtering and subtracting the baseline spectra observed with the I_2 flow off. The processed absorption signal from Figure 11 is shown in Figure 12. For this measurement, the small-signal gain gives a value of $[I^*]$-$[I]/2$ = -3.5 x 10^{12} molecules/cm^3, while the I^* emission observed by the near-infrared spectrometer gives $[I^*]$ = 1.7 x 10^{12} molecules/cm^3. Combination of these values gives [I] = 1.04 x 10^{13} molecules/cm^3, and $[I^*]/[I]$ = 0.16. In addition, $([I^*]+[I])/2$ = 6.05 x 10^{12} molecules/cm^3, in excellent agreement with the initial injected I_2 concentration. This consistency check also confirms the accuracy of the emission diagnostic. However, for the measured O yield (0.3) and the $O_2(a)$ yield observed in the presence of iodine, the equilibrium relationship gives a predicted ratio $[I^*]/[I]$ = 0.6, i.e. just above the inversion threshold of 0.5. This would correspond to an expected positive gain of 7 x 10^{-4} %/cm, which clearly disagrees with the measurements.

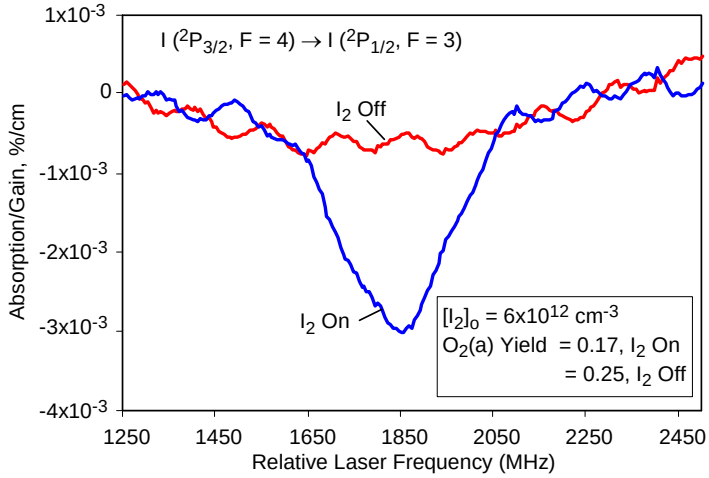

Figure 11. Single-pass tunable diode laser scans of atomic iodine line in net absorption, with and without the addition of I_2: 5% O_2/Ar, 70 W, 1.5 torr, 13 ms reaction time.

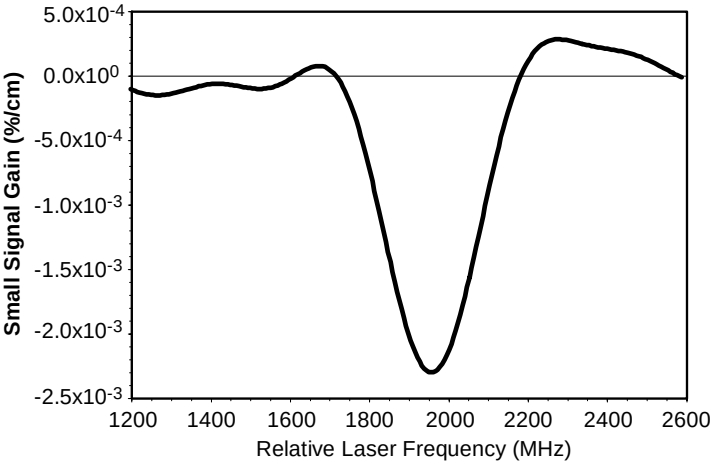

Figure 12. Processed tunable diode laser scan from the data in Figure 11, 5% O_2/Ar, 70 W, 1.5 torr, 13 ms reaction time.

Carroll et al.[6-8] also encountered $O_2(a)$ losses upon addition of I_2 to O_2/He discharge effluent streams in a supersonic discharge-flow system. They surmised that the effect was due to a global process whose net effect was rapid quenching of I^* by O. To negate this effect, they added NO_2 to the subsonic flow upstream of the iodine injection and the supersonic nozzle. The titration reaction

$$O + NO_2 \rightarrow NO + O_2 \qquad (8)$$

efficiently reduces [O]: if $[NO_2]_{added} < [O]$, then $[O]_{final} = [O]_{initial} - [NO_2]_{added}$; if $[NO_2]_{added} > [O]$, then all of the O is removed.[26,27] In addition, some of the NO combines with the remaining O to produce air-afterglow emission, providing a convenient and quantitative means to monitor the progress of the titration. As the NO_2 flow rate is increased from zero, the air afterglow intensity increases, passes through a maximum at $[NO_2]_o = [O]_{initial}/2$, and then decreases until it reaches zero at $[NO_2]_o$ $ $[O]_{initial}$. (However, we note that, for $[NO_2]_o \approx [O]_{initial}$, the reaction rate becomes second order, and it can take several ms to reduce [O] by two orders of magnitude.) When Carroll et al.[6,8] added NO_2 to their discharge effluent, they observed recovery of the $O_2(a)$ yield to its prior level, and concomitant increases in the $[I^*]/[I]$ ratio, including positive small-signal gain at reduced temperature in their supersonic flow section.

Accordingly, we added NO_2 through a fixed loop injector upstream of the I_2 injector, at flow rates giving $[NO_2]_o \sim [O]_{initial}$ as monitored via the air-afterglow intensity. These experiments used 5% O_2 in Ar at 1.5 torr, 350 K, and $[I_2]_o = 6 \times 10^{12}$ molecules/cm^3. As shown by the emission spectra in Figure 13, we observed essentially complete recovery of the initial $O_2(a)$ and a large increase in the I^* excitation. This was accompanied by decreased laser absorption, approaching transparency. However, as indicated in the figure, the resulting $[I^*]/[I]$ values were still below the inversion threshold of 0.5. With increasing $[NO_2]_{added}$, the remaining [O] became less than $2[I_2]_o$, so that O was the limiting reagent and I_2 was no longer fully dissociated. This resulted in decreasing $[I^*]$ and [I], however the ratio $[I^*]/[I]$ continued to increase. For the overtitrated condition $[O] \sim [I_2]_o$ and 7 ms reaction time, we observed ~50% dissociation of I_2, and the positive gain spectrum shown in Figure 14. As in Figure 12, this spectrum was processed by averaging 250 scans (~5 s), fast Fourier transform filtering, and subtraction of the baseline spectrum. Also shown in the figure is a Gaussian fit to the lineshape. The line-center small-signal gain for this case was $+8 \times 10^{-5}$ %/cm. The concentration determinations gave $O_2(a)$ yield = 0.25, $[I^*] = 2 \times 10^{12}$ molecules/cm^3, $[I] = 3.8 \times 10^{12}$ molecules/cm^3, and $[I^*]/[I] = 0.53$. Despite the extensive suppression of [O] in this measurement, the observed gain is well below the predicted value of 6×10^{-4} %/cm ($[I^*]/[I] = 0.7$) given by the equilibrium relationship. Nevertheless, these experiments demonstrate the feasibility of attaining positive gain on the $I^* \rightarrow I$ laser transition using $O_2(a)$ generated in a conventional, low-power microwave discharge in subsonic flow.

We have also obtained kinetic data on the loss of $O_2(a)$ caused by the injection of trace amounts of I_2. The $O_2(a)$ loss factor, $[O_2(a)]_o/[O_2(a)]$, increases with reaction time and with [O], with pseudo-first order loss rates on the order of 50 to 100 s^{-1}. Given the species and concentrations in the reactor, this loss cannot be caused by direct quenching of $O_2(a)$. However, the observed loss of $O_2(a)$ can occur through quenching of I^*, apparently by O. As the I^* concentration produced in Reaction (1) is depleted by quenching, $O_2(a)$ is converted to $O_2(X)$ as the equilibrium shifts. Carroll et al.[6,8] also observed this effect, and analyzed their data to infer an apparent $O + I^*$ quenching rate coefficient of 3.4×10^{-12} cm^3/molecule-s. This is considerably larger than the directly measured value of $<2 \times 10^{-12}$ cm^3/molecule-s reported by Heaven and coworkers for the isolated elementary reaction.[12]

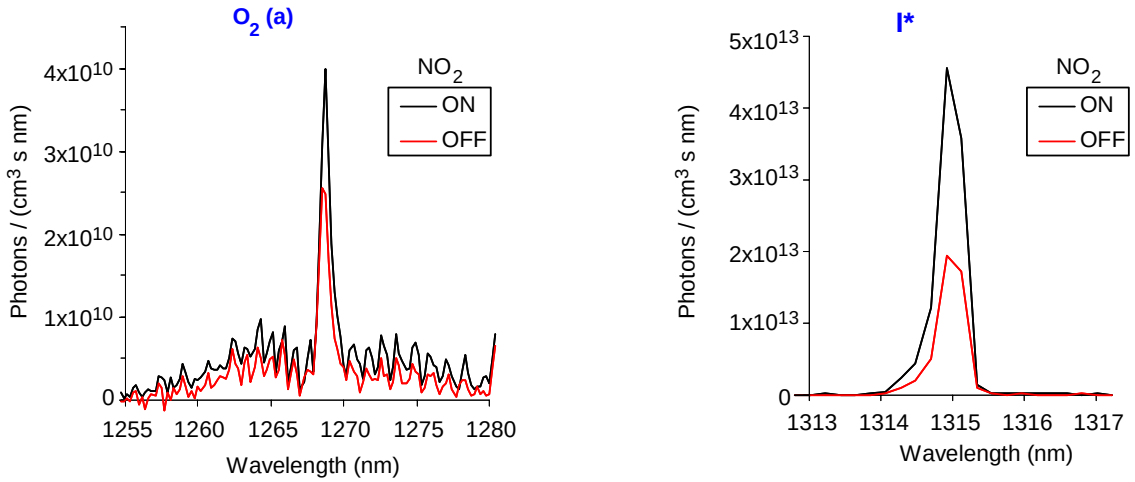

Figure 13. Effect of NO_2 addition on observed $O_2(a \rightarrow X)$ and $I^* \rightarrow I$ emission intensities: 5% O_2/Ar, 110 W, 1.5 torr, $[NO_2]_{added} = 0.95[O]_o$, $[O]/[O]_o = 1/20$. With NO_2 off: $O_2(a)$ yield = 0.15, $[I^*]/[I] = 0.13$. With NO_2 on: $O_2(a)$ yield = 0.25, $[I^*]/[I] = 0.36$.

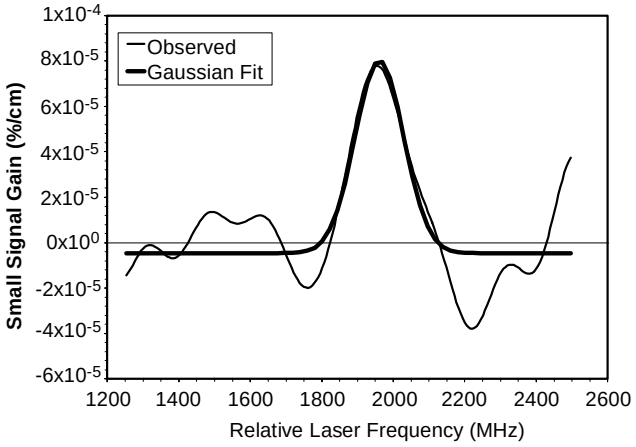

Figure 14. Processed tunable diode laser scan of atomic iodine line, showing net positive gain: 5% O_2/Ar, 70 W, 1.5 torr, 7 ms reaction time, NO_2 added, $[O] \cong [I_2]_o = 6 \times 10^{12}$ cm^{-3}, O_2(a) yield = 0.25. A Gaussian fit to the data is also shown.

We analyze the kinetics of O_2(a) loss by I^* quenching as follows. For simplicity, let the dissociation of I_2 by reactions of O with I_2 and IO be essentially instantaneous on our reaction time scale. The excitation and quenching of I^* can be described by three reactions:

$$O_2(a) + I \rightarrow O_2(X) + I^* \quad (R1)$$
$$O_2(X) + I^* \rightarrow O_2(a) + I \quad (-R1)$$
$$O + I^* \rightarrow O + I \quad (R2)$$

$$d[O_2(a)]/dt = k_{-1}[O_2(X)][I^*] - k_1[O_2(a)][I] \quad (9)$$

Equating the instantaneous production and loss rates of I^* (steady state approximation) gives the pseudo-first-order loss rate for O_2(a):

$$\frac{d\left(\ell n\left[O_2(a)\right]\right)}{dt} = -\frac{k_1 k_2 [I][O]}{k_{-1}\left[O_2\right] + k_2[O]} \quad (10)$$

This equation can be applied to observed O_2(a) loss rates for known [I], [O], and [O_2] to determine the value of k_2. Note that, since [I] > [I^*], the variation of [I] with reaction time due to I^* quenching is small.

A plot of the measured O_2(a) loss is shown in Figure 15, observed by adding I_2 through the sliding injector at different distances from the observation port. The measurements were made for 5.5% O_2 in Ar at 1.58 torr and 330 K, with a discharge power of 70 W and a flow velocity of 1280 cm/s. [I] was determined from the combination of I^* emission and I→I^* absorption measurements as described above: [I] = (7.9 " 1.0) x 10^{12} molecules/cm^3. The initial, unquenched [O_2(a)] was 6 x 10^{14} cm^{-3}. The slope of the line through the data points gives a pseudo-first-order O_2(a) loss rate of (97 " 15) s^{-1}. Solution of the above rate law for k_2 gives k_2 = (1.3 " 0.3(1σ)) x 10^{-11} cm^3/molecule-s. This is much larger than the upper bound measured for the elementary O + I^* quenching reaction,[12] indicating that our measurement represents a global overall process consisting of several elementary reactions.

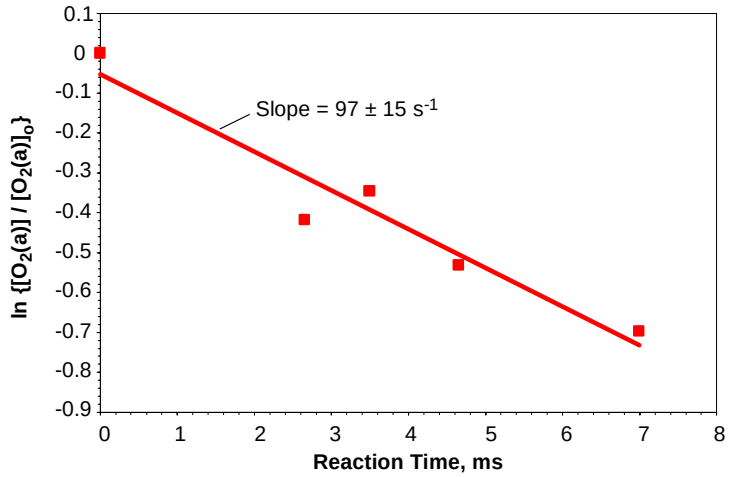

Figure 15. O_2(a) decay and first-order loss rate upon addition of I_2: $[I_2]_o = 4.7 \times 10^{12}$ cm^{-3}, 5.5% O_2/Ar, 70 W, 1.58 torr, $[O_2(a)]_0 = 6 \times 10^{14}$ cm^{-3}.

Using the techniques described above, we have determined [I^*]/[I] ratios for a range of reaction times and for discharge conditions giving a wide range of [O_2(a)]/[O_2(X)] ratios. The experimental conditions included: 1.5 torr, 5% and 50% O_2; 3 torr, 80% O_2; discharge power 40-120 W; reaction times 3-12 ms; and initial I_2 concentrations (0.5-1.3) x 10^{13} molecules/cm^3. Figure 16 summarizes the data in the form of a plot of [I^*]/[I] vs. [O_2(a)]/[O_2(X)]. Also shown on the plot is the equilibrium relationship from Equation (2), for 340 K. The experimental data span a range in [O_2(a)]/[O_2(X)] of 0.05 to 0.3, and all of the measured [I^*]/[I] values lie below the equilibrium values. The discrepancy between the data and Equation (2) increases with increasing [O_2(a)]/[O_2(X)], except for the case with NO_2 added. The observed trend does not appear to be strongly influenced by discharge power or reaction time. Possibly the data for the higher I_2 concentrations, all at [O_2(a)]/[O_2(X)] # 0.15 and 9 ms reaction time, trend closer to the line, however there are not enough data with different I_2 concentrations to conclude this with certainty. More systematic measurements are needed, particularly for dependence on [I_2]. However, it is clear from these data that the mechanism for I^* excitation and deactivation in discharged O_2 effluent streams is much more complex than previously thought.

V. Discussion: Kinetics and Mechanisms

Our observations of the microwave discharge yields of $O_2(a)$ and O, and of their trends with discharge conditions, are qualitatively consistent with predictions based on the chemical physics of the discharge. These data warrant more quantitative comparisons with discharge model predictions, which are in progress in our laboratory and will be reported elsewhere. Our preliminary analysis indicates that the calculated yields are most sensitive to the rate of electron loss to the walls associated with Debye shielding, and to the dissociation rates of $O_2(X)$ and $O_2(a)$. In addition, the effects of dissociative attachment and the O^- ion need to be carefully evaluated. For example, it appears that the role of O^- as an $O_2(a)$ sink is considerably muted if we consider the relatively low rate coefficient measured by Upschulte et al.[41] for the collisional detachment reaction:

$$O^- + O_2(a) \rightarrow O_3 + e^-, \quad k = 2.7 \times 10^{-11}\ cm^3/s \tag{11}$$

This value is an order of magnitude smaller than has been used in many previous discharge modeling calculations (e.g. Ref. 22). It also appears inevitable that increased $O_2(a)$ production will be accompanied by increased O production, which benefits I_2 dissociation but interferes with I^* excitation as discussed below. Our data suggest that the O production is considerably less than predicted from commonly accepted dissociation cross sections, and this point requires further examination. The so-called "mercury mirror" technique[1,2,41] provides an effective means for catalytic removal of O in small-volume discharge-flow systems, however this approach has an inherently limited surface/volume ratio and short coating lifetime, and is not practical for larger scale, high-throughput systems required to demonstrate lasing and power scaling.

The attainment of positive $I^* \rightarrow I$ gain from discharge-generated $O_2(a)$ in subsonic flow is a necessary step in the eventual development of a recyclable, electrically pumped iodine laser system. Our results confirm and complement recent observations of gain in supersonic flow by Carroll et al.[6-8] In addition, we have observed significant unexpected kinetic limitations: (1) an O-related quenching process that reduces $O_2(a)$ yield in the presence of trace amounts of added I_2, and (2) an unknown mechanism which suppresses $[I^*]/[I]$ for a given $O_2(a)$ yield.

The first process is consistent with a global reaction of the form $I^* + O \rightarrow I + O$, which results in net deactivation of $O_2(a)$. However, the global rate coefficient to account for our data is $\sim 10^{-11}$ cm^3/s, much larger than the upper bound of $<2 \times 10^{-12}$ cm^3/s measured for the isolated elementary $O + I^*$ reaction.[12] Our value is also larger than that of 3.4×10^{-12} cm^3/s determined by Carroll et al.[8] for the equivalent global process at 10 torr and much larger I_2 concentrations, $[I_2] \sim 10^{14}$ molecules/cm^3. This suggests the possibility of an overall quenching mechanism containing an inverse dependence on total-I concentration.

The second process is revealed by the difficulty of achieving positive gain even with 20-25% $O_2(a)$ yields, once the $O_2(a)$ loss mechanism was suppressed by reduction of [O]. The discrepancies between the observed and equilibrium $[I^*]/[I]$ values shown in Figure 16 are too large to be accounted for by uncertainties in the experimental data or in the Einstein coefficients. Our present data base is sufficient to establish the discrepancy, but more systematic dependencies on [O], $[I_2]$, and reaction time need to be examined in order to clearly identify the reaction mechanism responsible. In the following discussion, we consider some candidate hypotheses.

As discussed above, the expected active constituents of the oxygen discharge effluent stream are primarily $O_2(a)$ and O, with much smaller (and supposedly insignificant) amounts of O_3, $O_2(X,v)$, $O_2(b)$, and the more energetic (~4.5 eV) O_2 metastables. Thus the

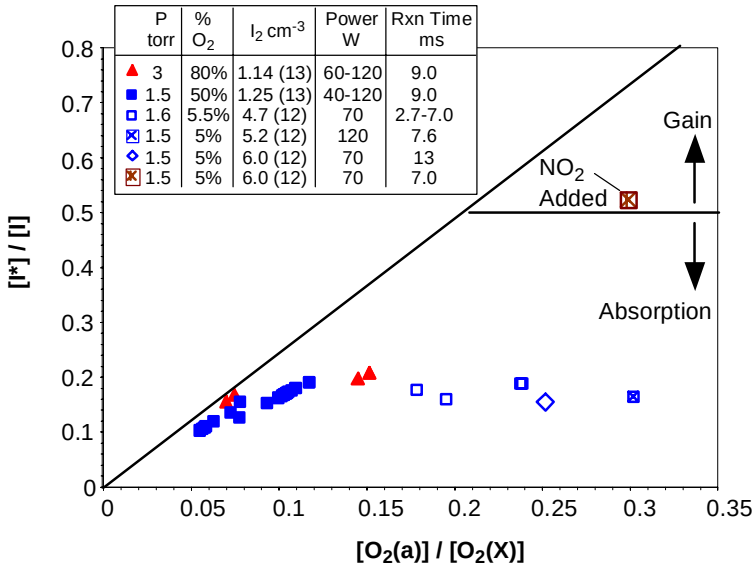

Figure 16. Observed dependence of $[I^*]/[I]$ on $[O_2(a)]/[O_2(X)]$, compared to the equilibrium relationship. Inversion of the atomic iodine state populations and positive gain occur for $[I^*]/[I] > 0.5$.

mechanistic possibilities are quite limited, unless one of the trace species is actually present at much larger concentration than expected from the known chemistry. We note that the energy of I^*, which lies 783 cal/mole below that of O_2(a,v=0), is 183 cal/mole *above* that of O_2(X,v=5).[42] This near-resonant relationship, 0.27kT at 350 K, suggests the possibility of a rapid energy exchange process, accompanied by O-atom deactivation of O_2(X,v=5):

$$I^* + O_2(X,v=0) \; W \; I + O_2(X,v=5) \tag{12}$$

$$O + O_2(X,v=5) \rightarrow O + O_2(X,v=0 \text{ to } 4) \tag{13}$$

The forward step of Reaction (12) is basically an exoergic branch of the $I^* + O_2$ quenching reaction, and the near-resonant forward and reverse reactions would proceed towards $K_{eq} \sim 1$, altering the overall equilibrium towards lower $[I^*]/[I]$ ratios. The deactivation of O_2(X,v=5) by O is likely to be efficient, $k \sim 10^{-11}$ cm^3/s,[15,39] resulting in net loss of I^*. At low total-I concentrations, Reaction (13) removes O_2(X,v=5) more rapidly than it can be converted back to I^* by Reaction (-12). At large total-I concentrations and/or low [O], Reaction (-12) competes effectively against Reaction (13), and I^* loss is reduced. Thus this mechanism incorporates an inverse dependence on total-I concentrations as suggested above. We note that, in the regime [O] >> [I], Reaction (-12) can be neglected, and the sum of Reactions (12) and (13) gives the net global reaction

$$I^* + O \rightarrow I + O$$

as inferred in our experiments and by Carroll et al.[8]

In order to examine the effect of this mechanism for our experimental conditions, we performed kinetics modeling calculations using the elementary reaction set in Table 1. The rate coefficient values in the table were taken from the literature, except for k_4, which was adjusted to give an O_2(a) loss rate similar to our observation. The calculations were performed for 5% O_2 in Ar at 1.5 torr, 350 K, with initial O_2(a) and O yields of 0.23 and 0.3, respectively, and $[I_2]_o = 6 \times 10^{12}$ molecules/cm^3. Calculations were performed with and without reduction of [O] by the NO_2 titration reaction. The predicted behavior of small-signal gain with reaction time is shown in Figure 17. The curves in Figure 17a were calculated for the conventional mechanism, i.e. by omitting Reactions 4 and 5 in Table 1 and setting $k_6 = 1 \times 10^{-11}$ cm^3/s as inferred from our O_2(a) loss data. This calculation indicates substantial positive gain upon suppression of [O] by a factor of 20, and is clearly incompatible with our measurements. The curves in Figure 17b were calculated for the full reaction set in Table 1, assuming $k_4 = 7 \times 10^{-12}$ cm^3/s. These curves illustrate the progressive increases in the small-signal gain as [O] is reduced, first by a factor of 20 and then by a factor of 100 so that $[O]_o = [I_2]_o$ as in the experiments. At the lowest [O], the gain at our typical measurement time of 7 ms is small and positive, $\sim 1 \times 10^{-4}$ %/cm, as we observe. With no O suppression, the computed first-order O_2(a) loss rate at 7 ms is 118 s^{-1}, and the I_2 dissociation is 100%, also in agreement with the observations. With O suppression to $[O]_o = [I_2]_o$, the O_2(a) loss rate at 7 ms is 33 s^{-1}, and the I_2 dissociation is 67%, both larger than measured. In addition, the computed [O] is rapidly removed by excess I_2, and is $<10^{11}$ molecules/cm^3 at >6 ms. We stress that, at this writing, the reaction mechanism in Table 1 represents a preliminary and unproven hypothesis,

Table 1. Hypothetical Reaction Mechanism

	k (350 K), cm^3/s	Reference
$O + I_2 \xrightarrow{1} IO + I$	1.5 (-10)	5
$O + IO \xrightarrow{2} O_2 + I$	1.4 (-10)	5
$O_2(a) + I \xrightarrow{3} O_2 + I^*$	$K_{EQ}\, k_{-3}$	2
$O_2 + I^* \xrightarrow{-3} O_2(a) + I$	$3.3 \times 10^{-11} - k_4$	2
$O_2 + I^* \xrightarrow{4} O_2(v=5) + I$	k_4	
$O_2(v=5) + I \xrightarrow{-4} O_2 + I^*$	$k_{-4} = k_4$	
$O_2(v=5) + O \xrightarrow{5} O_2 + O$	~ 1 (-11)	15, 39
$O + I^* \xrightarrow{6} O + I$	~ 1 (-12)	12

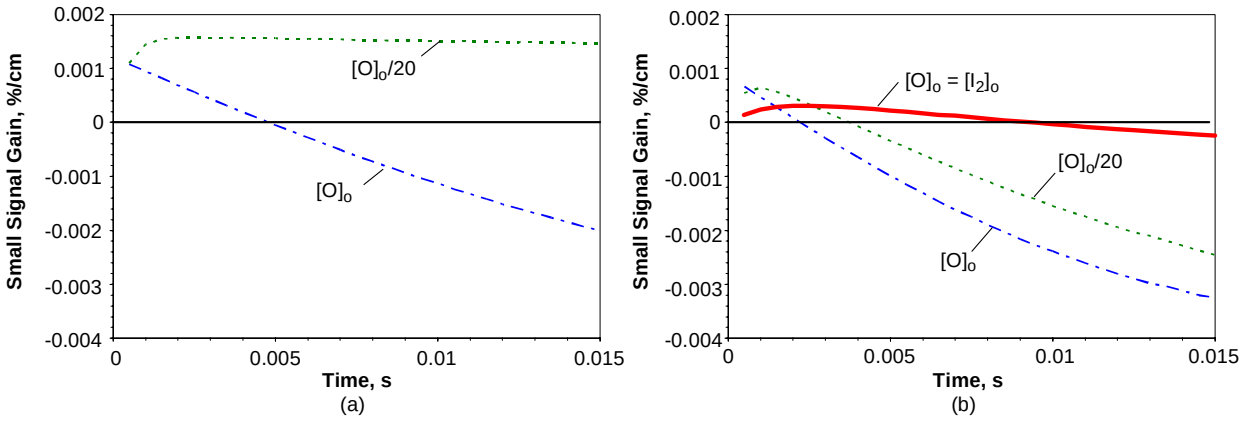

Figure 17. Dependence of small-signal gain on reaction time, computed for the reaction mechanism given in Table 1, 5% O_2/Ar, 1.5 torr, 350 K, initial $O_2(a)$ yield = 0.23, initial O yield = 0.3: (a) $k_4 = k_{-4} = k_5 = 0$, $k_6 = 1 \times 10^{-11}$ cm^3/s; (b) rate coefficients as given in Table 1 with $k_4 = 7 \times 10^{-12}$ cm^3/s.

which is qualitatively consistent with our data for a very specific set of experimental conditions. More comprehensive measurements and comparative modeling will be required to fully test this hypothetical reaction mechanism.

Possible contributions from O_3 and $O_2(v)$ seem unlikely but should be considered. If present in sufficient quantities, O_3 could alter the [I*]/[I] ratios through the reaction

$$O_3 + I \rightarrow IO + O_2 \ , \tag{14}$$

which may proceed with a larger rate coefficient for I^* than for I. This reaction would not deplete total I since the O + IO reaction would promptly regenerate I. If O_3 is formed only by three-body recombination of O and O_2, it is straightforward to calculate that its concentration in the flow reactor will be $<10^{12}$ molecules/cm^3 and therefore negligible. However, Copeland and co-workers[43,44] have shown that one of the 4.5 eV metastables of O_2, $O_2(A^3\Sigma,v)$, can react efficiently with $O_2(X)$ to form O_3:

$$O_2(A^3\Sigma_u^+,v) + O_2(X^3\Sigma_g^-) \rightarrow O_3 + O, \ k \cong 3 \times 10^{-11} \text{ cm}^3/\text{s} \tag{15}$$

This reactive property may also apply to the other nested 4.5 eV states, $O_2(A'^3\Delta_u)$ and $O_2(c^1\Sigma_u^-)$. $O_2(c)$ is excited in the discharge by electron impact with a rate coefficient of ~6×10^{-10} cm^3/s,[15] and we expect similar values for the other states. For our flow velocities, the $O_2(A,A',c)$ that exits the active discharge is quenched by O and O_2 within tens of microseconds, and much of this quenching could proceed through the potentially reactive channel with O_2. The O_3 concentrations formed by this mechanism could conceivably exceed 10^{13} molecules/cm^3, and thus could be a factor if the $I^* + O_3$ reaction occurs with a near-gas-kinetic rate coefficient. This question can be directly addressed through measurements of O_3 concentrations in the flow reactor.

Similarly, interference from vibrationally excited $O_2(v)$ must also be considered. $O_2(v)$ is formed efficiently in the discharge by electron impact excitation, $k \sim 10^{-9}$ cm^3/s,[15] however it should be rapidly quenched by O and walls downstream of the discharge. When O is reduced by the $O + NO_2$ titration reaction, $O_2(v)$ from the discharge and/or from the titration reaction,

$$O + NO_2 \rightarrow NO + O_2(v) \ , \tag{16}$$

may persist into the $O_2(a) + I$ reaction zone:

$$O_2(a,v) + I \ \text{W} \ I^* + O_2(X,v) \ . \tag{17}$$

The primary effect would be to reduce the energy defect between the right-hand and left-hand sides of the reaction, thus lowering the equilibrium constant and the $[I^*]/[I]$ ratio for a given $O_2(a)$ yield. This would limit the small-signal gain observed with suppressed [O]. We would expect to observe evidence of vibrationally excited $O_2(a,v)$ in

the emission spectra, however there is no clear evidence for this in our spectral data. This can be addressed by further experiments varying the flow times from the discharge and the NO_2 injector.

VI. Conclusions

We have used a microwave discharge-flow reactor and a comprehensive optical diagnostic suite to characterize the kinetics of I^* excitation and small-signal gain by electrically generated $O_2(a)$. The diagnostic suite provided independent measures of the concentrations of $O_2(a)$, $O_2(b)$, O, I_2, I^*, and I, all as functions of reaction time. Using discharge modeling predictions of the relevant electron-impact excitation and ionization rate coefficients, we identified and experimentally quantified a range of discharge conditions (low O_2 mole fractions, high E/N) giving $O_2(a)$ yields of 0.2 to 0.3. The results also indicate O yields of comparable magnitude, which are much smaller relative to the $O_2(a)$ yields than predicted from commonly accepted O_2 dissociation cross sections. Upon addition of the I_2 reagent at low concentrations, we found that the $O_2(a)$ concentration was reduced via an unexpected I^* quenching mechanism involving O produced in the discharge. When we reduced the O concentration by a factor of ~100 through titration with NO_2, we observed positive small-signal gain, in a subsonic flow at ~350 K. This observation is an important step in determining the feasibility of a microwave-driven hybrid electric oxygen-iodine laser. However, for all experimental conditions, we consistently observed small-signal gains which were much lower than expected from the conventional $O_2(a)/I^*$ equilibrium description. These results indicate the existence of one or more multi-step reaction mechanisms for quenching of I^* in the discharge effluent flow stream which have not previously been identified.

The discovery of an unknown I^* deactivation mechanism does not significantly impact the feasibility of an efficient hybrid electric oxygen-iodine laser, but rather prompts more systematic fundamental investigations to provide data and models required for scaling and optimizing the system. Indeed, our observation of positive gain in subsonic flow[9] was preceded by positive gain observations and successful laser power extraction in supersonic flow.[6-8] The small-signal gain observed in our subsonic flow experiments scales to 0.02%/cm for $[I_2]_o \sim 10^{15}$ cm^{-3}, indicating the potential for a viable subsonic laser. The combination of these emerging experimental results verifies the potential of the hybrid laser concept. We are continuing to pursue coupled kinetics experiments and modeling over a broader range of experimental parameters, both for the oxygen discharge kinetics and for the I^* excitation chemistry.

Acknowledgements

The authors appreciate many stimulating discussions with Wayne Solomon at University of Illinois Urbana-Champaign, David Carroll and Joseph Verdeyen at CU Aerospace, Michael Heaven at Emory University, Glenn Perram at the Air Force Institute of Technology, Gordon Hager and Timothy Madden at the Air Force Research Laboratory, and B. David Green and George Caledonia at Physical Sciences Inc. This research was funded by the Air Force Office of Scientific Research through a Multidisciplinary Research Initiative, prime contract F49620-01-1-0357, Dr. Michael Berman, contract monitor.

References

[1] Derwent, R.G. and Thrush, B.A., "Excitation of Iodine by Singlet Molecular Oxygen. Part 2. Kinetics of the Excitation of the Iodine Atoms," *Faraday Discuss. Chem. Soc.* 53, 162-171 (1972).

[2] Heidner, R.F., III, Gardner, C.E., Segal, G.I., and El-Sayed, T.M., "Chain-Reaction Mechanism for I_2 Dissociation in the $O_2(^1\Delta)$-I Atom Laser," *J. Phys. Chem.* 87, 2348-2360 (1983).

[3] McDermott, W., Pchelkin, N., Benard, D., and Bousek, R., "An Electronic Transition Chemical Laser," *Appl. Phys. Lett.* 32, 469 (1978).

[4] Hager, G.D., Watkins, L.J., Meyer, R.K., Johnson, D.E., Bean, L.J., and Loverro, D.L., "A Supersonic Chemical Oxygen-Iodine Laser," AFWL-TR-87-45, Air Force Weapons Laboratory, Kirtland AFB, New Mexico, January 1988.

[5] Payne, W.A., Thorn, R.P., Jr., Nesbitt, F.L., and Stief, L.J., "Rate Constant for the Reaction of $O(^3P)$ with IO at T = 298 K," *J.Phys.Chem. A* 102, 6247-6250 (1998).

[6] Carroll, D.L., Verdeyen, J.T., King, D.M., Zimmerman, J.W., Laystrom, J.K., Woodard, B.S., Richardson, N., Kittell, K., Kushner, M.J., and Solomon, W.C., "Measurement of Positive Gain on the 1315 nm Transition of Atomic Iodine Pumped by $O_2(a^1\Delta)$ Produced in an Electric Discharge," *Appl. Phys. Lett.* 85, 1320-1322 (2004).

[7] Carroll, D.L., Verdeyen, J.T., King, D.M., Zimmerman, J.W., Laystrom, J.K., Woodard, B.S., Benavides, G.F., Kittell, K., Stafford, D.S., Kushner, M.J., and Solomon, W.C., *Appl. Phys. Lett.* 86, 111104 (2005).

[8] Carroll, D.L., Verdeyen, J.T., King, D.M., Zimmerman, J.W., Laystrom, J.K., Woodard, B.S., Benavides, G.F., Kittell, K., and Solomon, W.C., *IEEE J. Quantum Electron.* 41, 213-223 (2005).

[9] Rawlins, W.T., Lee, S., Kessler, W.J., and Davis, S.J., "Observations of Gain on the I($^2P_{1/2}\rightarrow{}^2P_{3/2}$) Transition by Energy Transfer from $O_2(a^1\Delta_g)$ Generated by a Microwave Discharge in a Subsonic Flow Reactor," *Appl. Phys. Lett.* 86, 051105 (2005).

[10] Rawlins, W.T., Davis, S.J., Lee, S., Silva, M.L., Kessler, W.J., and Piper, L.G., "Optical Diagnostics and Kinetics of Discharge-Initiated Oxygen-Iodine Energy Transfer," AIAA-2003-4032, 34th AIAA Plasmadynamics and Lasers Conference, Orlando, FL, June 2003.

[11] Rawlins, W.T., Lee, S., Kessler, W.J., Oakes, D.B., Piper, L.G., and Davis, S.J., "Spectroscopic Studies of a Prototype Electrically Pumped COIL System," SPIE 5334, Paper No. 12 (2004).

[12] Han, J., Tinney, S.P., and Heaven, M.C., "I^* Kinetics of Relevance to Discharge Driven COIL Systems," Proc. SPIE 5448, 261-268 (2004).

[13] Fehsenfeld, F.C., Evenson, K.M., and Broida, H.P., "Microwave Discharge Cavities Operating at 2450 MHz," *Rev. Sci. Instrum.* 36, 294-298 (1965).

[14] Kaufman, F., "The Production of Atoms and Simple Free Radicals in Glow Discharges," *Adv. Chem. Ser.* 80, 29-47 (1969).

[15] Rawlins, W.T., Caledonia, G.E., and Armstrong, R.A., "Dynamics of Vibrationally Excited Ozone Formed by Three-Body Recombination. II. Kinetics and Mechanism," *J. Chem. Phys.* 87, 5209-5221 (1987).

[16] Morgan, W.L. and Penetrante, B.M., "ELENDIF: A Time-Dependent Boltzmann Solver for Partially Ionized Plasmas," *Computer Physics Communications* 58, 127-152 (1990).

[17] Frost, L.S. and Phelps, A.V., "Momentum-Transfer Cross Sections for Slow Electrons in He, Ar, Kr, and Xe from Transport Coefficients," *Phys. Rev. A* 136, 1538 (1969).

[18] Lawton, S.A., and Phelps, A.V., "Excitation of the $b^1\Sigma_g^+$ State of O_2 by Low Energy Electrons," *J. Chem. Phys.* 69, 1055 (1978).

[19] Tachibana, K., and Phelps, A.V., "Excitation of the O_2 ($a^1\Delta_g$) State by Low Energy Electrons," *J. Chem. Phys.* 75, 3315 (1981).

[20] Phelps, A.V., private communication, ftp://jila.colorado.edu/collision_data/.

[21] Franklin, R.N., "The Role of $O_2(a^1\Delta_g)$ Metastables and Associative Detachment in Discharges in Oxygen," *J. Phys. D: Appl. Phys.* 34, 1834-1839 (2001).

[22] Stafford, D.S. and Kushner, M.J., "$O_2(^1\Delta)$ Production in He/O_2 Mixtures in Flowing Low Pressure Plasmas," *J. Appl. Phys.* 96, 2451-2465 (2004).

[23] Davis, S.J. and Hanko, L., "An I_2 Flow Rate Diagnostic for the Oxygen Iodine Laser," Laser Digest, AFWL-TR-79-104, Air Force Weapons Laboratory, Kirtland AFB, New Mexico, 1979.

[24] Davis, S.J., Allen, M.G., Kessler, W.J., McManus, K.R., Miller, M.F., and Mulhall, P.A., "Diode Laser-Based Sensors for Chemical Oxygen Iodine Lasers," SPIE 2702, 195 (1996).

[25] Allen, M.G., Carleton, K.L., Davis, S.J., Kessler, W.J., Otis, C.E., Palombo, D.A., and Sonnenfroh, D.M., "Ultra-Sensitive Dual-Beam Absorption and Gain Spectroscopy: Applications for Near-IR and Visible Diode Laser Sensors," *Appl. Opt.* 34, 3240 (1995).

[26] Kaufman, F., "The Air Afterglow and Its Use in the Study of Some Reactions of Atomic Oxygen," *Proc. Roy. Soc. A* 247, 123-139 (1958).

[27] Kaufman, F., "Reactions of Oxygen Atoms," *Progress in Reaction Kinetics* 1, 1-39 (1961).

[28] Piper, L.G., "The Rate Coefficient for Quenching N(^{2}D) by O(^{3}P)," *J. Chem. Phys.* 91, 3516-3524 (1989).

[29] Herzberg, G., *Molecular Spectra and Molecular Structure I. Spectra of Diatomic Molecules* (Van Nostrand, New York, 1951).

[30] Newman, S.M., Lane, I.C., Orr-Ewing, A.J., Newnham, D.A., and Ballard, J., "Integrated Absorption Intensity and Einstein Coefficients for the O_2 $a^1\Delta_g - X^3\Sigma_g^-(0,0)$ Transition: A Comparison of Cavity Ringdown and High Resolution Fourier Transform Spectroscopy with a Long-Path Absorption Cell," *J. Chem. Phys.* 110, 10749-10757 (1999).

[31] Lafferty, W.J., Solodov, A.M., Lugez, C.L., and Fraser, G.T., "Rotational Line Strengths and Self-Pressure-Broadening Coefficients for the 1.27 μm, $a^1\Delta_g - X^3\Sigma_g^-$, v = 0-0 Band of O_2," *Appl. Opt.* 37, 2264-2270 (1998).

[32] Engleman, R., Jr., Palmer, B.A., and Davis, S.J., "Transition Probability and Collision Broadening of the 1.3−μm Transition of Atomic Iodine," *J. Opt. Soc. Am.* 73, 1585-1589 (1983).

[33] Tellinghuisen, J., "Resolution of the Visible-Infrared Absorption Spectrum of I_2 into Three Contributing Transitions," *J. Chem. Phys.* 58, 2821-2834 (1973).

[34] Tellinghuisen, J., "Transition Strengths in the Visible-Infrared Absorption Spectrum of I_2," *J. Chem. Phys.* 76, 4736-4744 (1982).

[35] Black, G. and Slanger, T.G., "Production of $O_2(a^1\Delta_g)$ by Oxygen Recombination on a Pyrex Surface," *J. Chem. Phys.* 74, 6517-6519 (1981).

[36] Marinelli, W.J. and Green, B.D., "Collisional Quenching of Atoms and Molecules on Spacecraft Thermal Protection Surfaces," AIAA Paper 88-2667 (1988).

[37] Lee, L.C. and Slanger, T.G., "Observations on O(^{1}D→^{3}P) and $O_2(b^1\Sigma_g^+\rightarrow X^3\Sigma_g^-)$ Following O_2 Photodissociation," *J. Chem. Phys.* 69, 4053-4060 (1978).

[38] Slanger, T.G. and Black, G., "Interactions of $O_2(b^1\Sigma_g^+)$ with O(^{3}P) and O_3," *J. Chem. Phys.* 70, 3434-3438 (1979).

[39] Gelb, A.H. and Rawlins, W.T., "Relaxation of Vibrationally Excited Oxygen Molecules by Collision with Oxygen Atoms," Physical Sciences Inc. TR-567, 1986. This unpublished report describes classical trajectory calculations for the $O + O_2(v)$ interaction using the theoretical O_3 potential surface of J.N. Murrell and coworkers: A.J. Stace and J. N. Murrell, *J. Chem. Phys.* 68, 3078 (1978); A.J.C. Varandas and J. N. Murrell, *Chem. Phys. Lett.* 88, 1 (1982).

[40] Cosby, P.C., "Electron-Impact Dissociation of Oxygen," *J. Chem. Phys.* 98, 9560-9569 (1993).

[41] Upschulte, B.L., Marinelli, W.J., and Green, B.D., "Reactions of $O_2(a^1\Delta_g)$ with O^- and O_2^-," *J. Phys. Chem.* 98, 837-842 (1994).

[42] Krupenie, P.H., "The Spectrum of Molecular Oxygen," *J. Phys. Chem. Ref. Data* 1, 423-534 (1972).

[43] Copeland, R.A., "Laser Double Resonance Study of Collisional Removal of $O_2(A^3\Sigma_u^+,v=7)$ with O_2," *J. Chem. Phys.* 100, 744 (1994).

[44] Knutsen, K., Dyer, M.J., and Copeland, R.A., "Laser Double-Resonance Study of the Collisional Removal of $O_2(A^3\Sigma_u^+,v=6,7,9)$ with O_2, N_2, CO_2, Ar, and He," *J. Chem. Phys.* 101, 7415-7422 (1994).